SICE Annual Conference 2010
August 18-21, 2010, The Grand Hotel, Taipei, Taiwan

Visual Servoing with Quick Eye-Vergence to Enhance Trackability and Stability

Fujia Yu, Wei Song and Mamoru Minami

Abstract— **Visual servoing methods for hand-eye configuration are vulnerable for hand's dynamical oscillation, since nonlinear dynamical effects of whole manipulator stand against the stable tracking ability (trackability). Our proposal to solve this problem is that the controller for visual servoing of the hand and the one for eye-vergence should be separated independently based on decoupling each other, where the trackablity is verified by Lyapunov analysis. Then the effectiveness of the decoupled hand & eye-vergence visual servoing method is evaluated through simulations incorporated with actual dynamics of 7-DoF robot with additional 3-DoF for eye-vergence mechanism.**

I. Introduction

Visual servoing can be classified into three major groups by its methods: position-based, image-based and hybrid visual servoing [3]. In most image-based researches they concentrated on a planar object [4], [5], while in the hybrid controller the object is always static [6]. A hand-eye configuration has a merit of the ability choosing the viewpoint adaptively instead of the tendency being unstable during servoing motion due to hand's dynamical oscillation. Thus enhancing both the camera's tracking ability and robot's servoing stability is inherent hazard for hand-eye configuration, since they deteriorate each other in visual servoing motion. Also keeping suitable viewpoint is important for pose estimation to track the target precisely. If a pose measurement system can provide servoing controller with correct pose without time-delay, it can improve the stability of servoing dynamics since it is common sense that the time-delay existing in feedback mechanism may mess up closed-loop stability. Some methods are proposed to improve observation, like using stereo camera [7], multiple cameras [8], and two cameras: with one fixed on the end-effector, and the other done in the workspace [9]. However, these methods to give different views to observe the object by only increasing the number of cameras remain in less adaptive for changing environment.

On the other hand, a fixed-hand-eye system has some disadvantages, making the observing ability deteriorated depending on the relative geometry of the camera and the target. Such as: the robot cannot observe the object well when it is near the cameras (Fig. 1 (a)), small intersection of the possible sight space of the two cameras (Fig. 1 (b)), and the image of the object cannot appear in the center of both cameras, so we could not get clear image information of target and its periphery, reducing the pose measurement accuracy (Fig. 1 (c)). To solve the problems above, in this paper, we give the cameras an ability to rotate themselves to see target at center of the images. Thus it is possible to change the pose of the cameras in order to observe the object better, as it is shown in Fig. 2, enhancing the measurement accuracy in trigonometric calculation and peripheral distortion of camera lens by observing target at the center of lens. Moreover, recent researches on visual servoing are limited generally in a swath of tracking an object while keeping a certain constant distance [7], [10], [11]. But the final objective of visual servoing lies in approaching the end-effector to a target and then work on it, like grasping. In this case, the desired relation between the cameras and the object is time varying, so such rotational camera system in Fig. 2 is required to keep suitable viewpoint all the time during the visual servoing application.

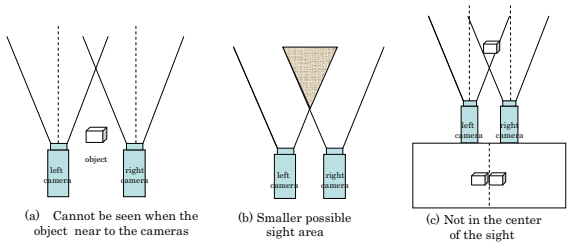

Fig. 1. Disadvantage of fix camera system

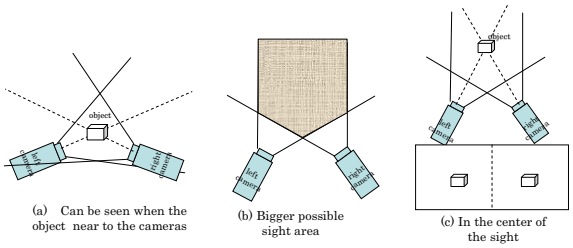

Fig. 2. Advantage of Eye-vergence system

In visual servoing application, it is important to keep the object in the visual eye sight to make the visual feed back not be severed to keep stable closed-loop dynamical motion. If the camera lose the sight of target, its pose cannot be measured, that means, the visual feedback is cut, and the robot may fall in some unexpected motion, being dangerous. As it is shown in Fig. 3 (a), in visual servoing system the

Fujia Yu is with Department of Human and Artificial Intelligence Systems, Graduate School of Engineering, University of Fukui, Fukui, 910-8507, Japan yufujia@sys.okayama-u.ac.jp , Wei Song is with School of Mechatronics Engineering and Automation, University of Shanghai, 200-072, Shanghai, China songwei5726@hotmail.com Mamoru Minami is with Graduate School of Natural Science and Technology, Okayama University, Okayama, 700-8530, Japan minami@sys.okayama-u.ac.jp

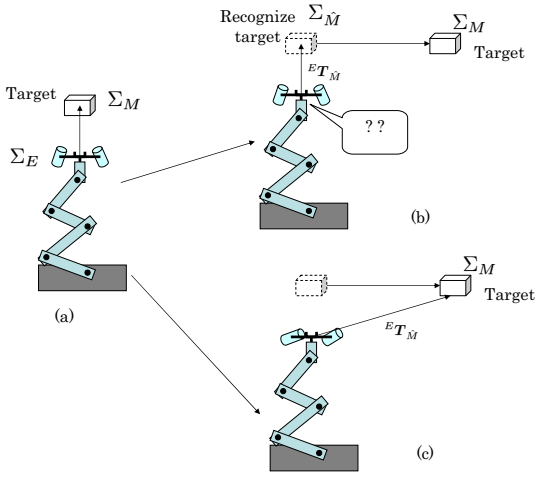

Fig. 3. Dynamics advantage of Eye-vergence system

cameras can keep staring at the object at first in (a), but when the target moves so fast that the manipulator can not catch up the speed of the target because of the big mass of whole manipulator itself, then the object may disappear in the sight of the cameras, resulting in that the visual feedback of the system is cut as shown in (b), loosing feedback information that appears most dangerous. So in visual servoing system it is very important to keep the camera tracking the target. A system with high tracking ability also has better security and validity. To realize this stable tracking ability against quick and unknown motion of the target, we propose to control the cameras and the manipulator separately. Because of the small mass and inertia moment of the cameras, it can track the target better, as in Fig. 3 (c), like animals tracks target with eye motion before rotate their heads to the target to improve dynamical tracking ability.

To evaluate the observation of the camera, we put forward a concept of trackability. This concept has been used in [12], where trackability is defined as a kinematic function of singular value of Jacobian matrix connecting hand's velocities and angular joint velocities, ignoring the relationship between the hand and the target objects, including the both dynamical motion of the target and the manipulator, which seems to be essential for evaluating the eye-vergence visual servoing. Then we define a new concept of trackability to appreciate our visual servoing proposal introduced in the next paragraph.

In this report, we present a hand & eye-vergence dual visual servoing system with a stability analysis of Lyapunov method, guaranteeing that both the tracking pose errors of hand and eye-vergence converge to zero. As shown in Fig. 4, the proposed method includes two loops: a loop for conventional visual servoing that direct a manipulator toward a target object and an inner loop for active motion of binocular camera for accurate and broad observation of the target object. We set relatively high gain to the eye-vergence controller to put the priority to the 3D pose tracking to improve the system trackability.

The effectiveness of the proposed hand & eye-vergence

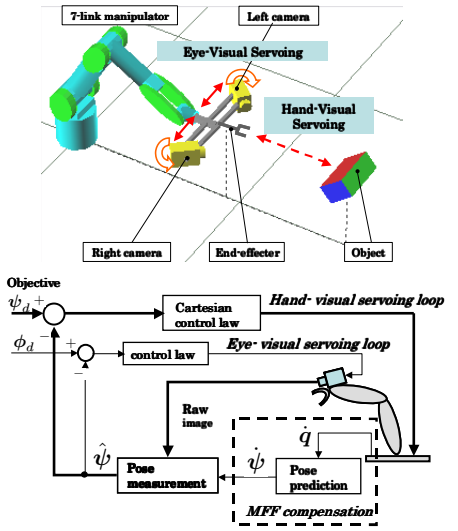

Fig. 4. Hand & Eye Visual servo system

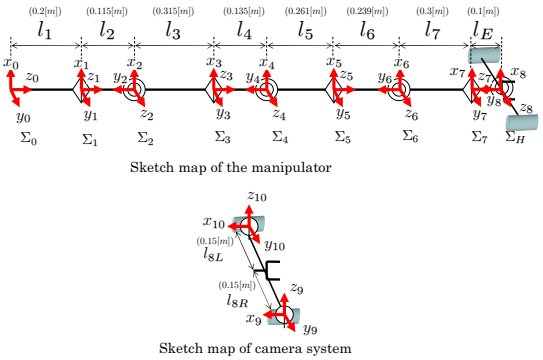

Fig. 5. Sketch map of the eye-vergence system

dual visual servoing will be evaluated through simulations incorporated with actual dynamics of 7-DoF robot with additional 3-DoF for eye-vergence mechanism of left and right camera's motion. We discuss the performance of the proposed system on the view points of how the new idea improve the stability and trackability against quick motion of the target.

II. Hand & Eye Visual Servoing

A. Experiment circumstance

The Mitsubishi PA-10 robot arm is a 7-DoF robot arm manufactured by Mitsubishi Heavy Industries.

The general equation of motion of manipulator is

$$\boldsymbol{M}(\boldsymbol{q}_E)\ddot{\boldsymbol{q}}_E + \boldsymbol{h}(\boldsymbol{q}_E, \dot{\boldsymbol{q}}_E) + \boldsymbol{g}(\boldsymbol{q}_E) + \boldsymbol{d}(\dot{\boldsymbol{q}}_E) = \boldsymbol{\tau}_E, \quad (1)$$

where, $\boldsymbol{q}_E$: the joint displacement and $\boldsymbol{q}_E = [q_1, q_2, \cdots, q_7]^T$, $\boldsymbol{\tau}_E$: the joint driving force and $\boldsymbol{\tau}_E = [\tau_1, \tau_2, \cdots, \tau_7]^T$, $\boldsymbol{M}(\boldsymbol{q}_E)$: the inertia matrix, $\boldsymbol{h}(\boldsymbol{q}_E, \dot{\boldsymbol{q}}_E)$: the vector representing the centrifugal and coriolis forces, $\boldsymbol{g}(\boldsymbol{q}_E)$: the vector representing the gravity load, $\boldsymbol{d}(\dot{\boldsymbol{q}}_E)$: the vector representing the frictional force. Here, we assume $\boldsymbol{d}(\dot{\boldsymbol{q}}_E) = \boldsymbol{0}$. Two rotatable cameras mounted on the end-effector are FCB-1X11A manufactured

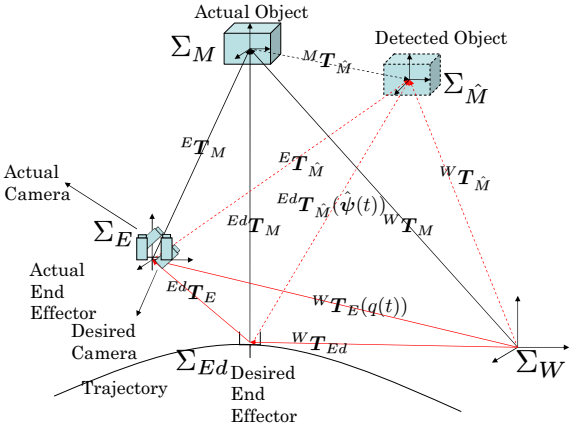

Fig. 6. Motion of the end-effector and object

by Sony Industries. The frame frequency of stereo cameras is set as 33fps. The image processing board, CT-3001, receiving the image from the CCD camera is connected to the DELL WORKSTATION PWS650 (CPU: Xeon, 2.00 GHz) host computer. The structure of the manipulator and the cameras are shown in Fig. 5.

B. Desired-trajectory generation

As shown in Fig. 6, the world coordinate frame is denoted by Σ_W, the target coordinate frame is denoted by Σ_M, and the desired and actual end-effector coordinate frame is denoted by Σ_{Ed}, Σ_E separately. The desired relative relation between the target and the end-effector is given by Homogeneous Transformation as ${}^{Ed}\boldsymbol{T}_M$, the relation between the target and the actual end-effector is given by ${}^{E}\boldsymbol{T}_M$, then the difference between the desired end-effector pose Σ_{Ed} and the actual end-effector pose Σ_E is denoted as ${}^{E}\boldsymbol{T}_{Ed}$, ${}^{E}\boldsymbol{T}_{Ed}$ can be decribed by:

$$ {}^{E}\boldsymbol{T}_{Ed}(t) = {}^{E}\boldsymbol{T}_M(t)\,{}^{Ed}\boldsymbol{T}_M^{-1}(t) \qquad (2) $$

(2) is a general deduction that satisfies arbitrary object motion ${}^{W}\boldsymbol{T}_M(t)$ and arbitrary visual servoing objective ${}^{Ed}\boldsymbol{T}_M(t)$. However, the relation ${}^{E}\boldsymbol{T}_M(t)$ is only observed by cameras using the on-line model-based recognition method and 1-step GA [7], [15]. Let $\Sigma_{\hat{M}}$ denote the detected object, there always exist an error between the actual object Σ_M and the detected one $\Sigma_{\hat{M}}$. So in visual servoing, (2) will be rewritten based on $\Sigma_{\hat{M}}$ that includes the error ${}^{M}\boldsymbol{T}_{\hat{M}}$, as

$$ {}^{E}\boldsymbol{T}_{Ed}(t) = {}^{E}\boldsymbol{T}_{\hat{M}}(t)\,{}^{Ed}\boldsymbol{T}_{\hat{M}}^{-1}(t), \qquad (3) $$

where ${}^{E}\boldsymbol{T}_{\hat{M}} = {}^{E}\boldsymbol{T}_M$ determined by the given visual servoing objective. Differentiating (3) with respect to time yields

$$ {}^{E}\dot{\boldsymbol{T}}_{Ed}(t) = {}^{E}\dot{\boldsymbol{T}}_{\hat{M}}(t)\,{}^{\hat{M}}\boldsymbol{T}_{Ed}(t) + {}^{E}\boldsymbol{T}_{\hat{M}}(t)\,{}^{\hat{M}}\dot{\boldsymbol{T}}_{Ed}(t), \qquad (4) $$

Differentiating Eq. (4) with respect to time again

$$ {}^{E}\ddot{\boldsymbol{T}}_{Ed}(t) = {}^{E}\ddot{\boldsymbol{T}}_{\hat{M}}(t)\,{}^{\hat{M}}\boldsymbol{T}_{Ed}(t) + 2\,{}^{E}\dot{\boldsymbol{T}}_{\hat{M}}(t)\,{}^{\hat{M}}\dot{\boldsymbol{T}}_{Ed}(t) + {}^{E}\boldsymbol{T}_{\hat{M}}(t)\,{}^{\hat{M}}\ddot{\boldsymbol{T}}_{Ed}(t), \qquad (5) $$

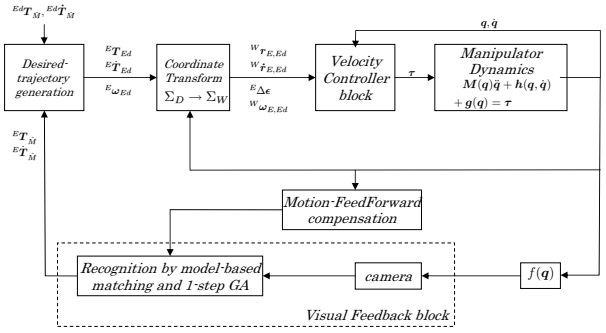

Fig. 7. Block diagram of the hand visual servoing system

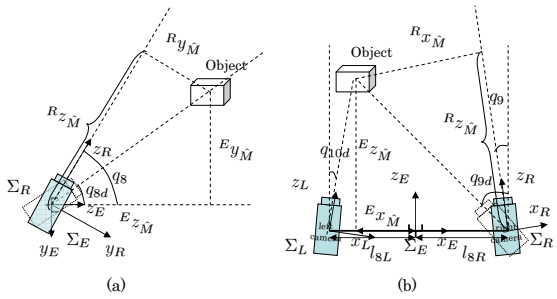

Fig. 8. Calculation of tilt and pan angles

Where ${}^{\hat{M}}\boldsymbol{T}_{Ed}$, ${}^{\hat{M}}\dot{\boldsymbol{T}}_{Ed}$, ${}^{\hat{M}}\ddot{\boldsymbol{T}}_{Ed}$ are given as the desired visual servoing objective. ${}^{E}\boldsymbol{T}_{\hat{M}}$, ${}^{E}\dot{\boldsymbol{T}}_{\hat{M}}$, ${}^{E}\ddot{\boldsymbol{T}}_{\hat{M}}$ can be observed by cameras. As shown in Fig. 6, there are two errors that we have to decrease to $\mathbf{0}$ in the visual servoing process. First one is the error between the actual object and the detected one, ${}^{M}\boldsymbol{T}_{\hat{M}}$, and the other is the error between the desired end-effector and the actual one, ${}^{E}\boldsymbol{T}_{Ed}$. In our research, the error of ${}^{M}\boldsymbol{T}_{\hat{M}}$ is decreased by on-line recognition method of 1-step GA, MFF compensation method and the eye-vergence camera system, and the error of ${}^{E}\boldsymbol{T}_{Ed}$ can be decreased by the hand visual servoing controller.

C. Hand & Eye Visual Servoing Controller

The block diagram of our proposed hand & eye-vergence visual servoing controller is shown in Fig. 4. The hand-visual servoing is the outer loop. A detailed block diagram of hand visual servoing control is depicted in Fig.7. Based on the above analysis of the desired-trajectory generation, the desired hand velocity ${}^{W}\dot{\boldsymbol{r}}_d$ is calculated as,

$$ {}^{W}\dot{\boldsymbol{r}}_d = \boldsymbol{K}_{P_p}\,{}^{W}\boldsymbol{r}_{E,Ed} + \boldsymbol{K}_{V_p}\,{}^{W}\dot{\boldsymbol{r}}_{E,Ed}, \qquad (6) $$

where ${}^{W}\boldsymbol{r}_{E,Ed}$, ${}^{W}\dot{\boldsymbol{r}}_{E,Ed}$ are given by transforming ${}^{E}\boldsymbol{T}_{Ed}$ and ${}^{E}\dot{\boldsymbol{T}}_{Ed}$ from Σ_E to Σ_W. $\boldsymbol{K}_{P_p}$ and $\boldsymbol{K}_{V_p}$ are positive definite matrix to determine PD gain.

The desired hand angular velocity ${}^{W}\boldsymbol{\omega}_d$ is calculated as,

$$ {}^{W}\boldsymbol{\omega}_d = \boldsymbol{K}_{P_o}\,{}^{W}\boldsymbol{R}_E\,{}^{E}\Delta\boldsymbol{\epsilon} + \boldsymbol{K}_{V_o}\,{}^{W}\boldsymbol{\omega}_{E,Ed}, \qquad (7) $$

where ${}^{E}\Delta\boldsymbol{\epsilon}$ is the quaternion error that from the recognition result directly, and ${}^{W}\boldsymbol{\omega}_{E,Ed}$ can be calculated by transform-

ing ${}^{E}\boldsymbol{T}_{Ed}$ and ${}^{E}\dot{\boldsymbol{T}}_{Ed}$ from Σ_E to Σ_W. Also, $\boldsymbol{K}_{P_o}$ and $\boldsymbol{K}_{V_o}$ are suitable feedback matrix gains.

The desired joint variable $\dot{\boldsymbol{q}}_d$ is obtained by

$$\dot{\boldsymbol{q}}_d = \boldsymbol{J}^{+}(\boldsymbol{q}) \begin{bmatrix} {}^{W}\dot{\boldsymbol{r}}_d \\ {}^{W}\boldsymbol{\omega}_d \end{bmatrix}. \tag{8}$$

where $\boldsymbol{J}^{+}(\boldsymbol{q})$ is the pseudoinverse matrix of $\boldsymbol{J}(\boldsymbol{q})$, and $\boldsymbol{J}^{+}(\boldsymbol{q}) = \boldsymbol{J}^{T}(\boldsymbol{J}\boldsymbol{J}^{T})^{-1}$. The hardware control system of the velocity-based servo system of PA10 is expressed as

$$\boldsymbol{\tau} = \boldsymbol{K}_{SP}(\dot{\boldsymbol{q}}_d - \dot{\boldsymbol{q}}) + \boldsymbol{K}_{SI}\int_0^t (\dot{\boldsymbol{q}}_d - \dot{\boldsymbol{q}})dt \tag{9}$$

where $\boldsymbol{K}_{SP}$ and $\boldsymbol{K}_{SI}$ are symmetric positive definite matrix to determine PI gain.

The eye-vergence visual servoing is the inner loop of the visual servoing system shown in Fig. 4. In this paper, we use two pan-tilt cameras for eye-vergence visual servoing. Here, the positions of cameras are supposed to be fixed on the end-effector. For camera system, q_8 is tilt angle, q_9 and q_{10} are pan angles, and q_8 is common for both cameras. As it is shown in Fig. 8, ${}^{E}x_{\hat{M}}$, ${}^{E}y_{\hat{M}}$, ${}^{E}z_{\hat{M}}$ express position of the detected object in the end-effector coordinate. The desired angle of the camera joints are calculated by:

$$q_{8d} = atan2({}^{E}z_{\hat{M}}, {}^{E}y_{\hat{M}}) \tag{10}$$
$$q_{9d} = atan2({}^{E}z_{\hat{M}}, -l_{8R} + {}^{E}x_{\hat{M}}) \tag{11}$$
$$q_{10d} = atan2({}^{E}z_{\hat{M}}, l_{8L} + {}^{E}x_{\hat{M}}) \tag{12}$$

where $l_{8L} = l_{8R} = 120[mm]$ that is the camera location. We set the center line of the camera as the z axis of each camera coordinate, so the object will be in the center of the sight of the right camera when ${}^{R}x_{\hat{M}} = 0$ and ${}^{R}y_{\hat{M}} = 0$, ${}^{R}x_{\hat{M}}$, ${}^{R}y_{\hat{M}}$, ${}^{R}z_{\hat{M}}$ express the position of the detected object in the right camera coordinate. While the object position relative to the cameras are:

$$\frac{{}^{R}y_{\hat{M}}}{{}^{R}z_{\hat{M}}} = tan(q_{8d} - q_8) \tag{13}$$
$$\frac{{}^{R}x_{\hat{M}}}{{}^{R}z_{\hat{M}}} = tan(q_{9d} - q_9) \tag{14}$$
$$\frac{{}^{L}x_{\hat{M}}}{{}^{L}z_{\hat{M}}} = tan(q_{10d} - q_{10}) \tag{15}$$

Here we can use the relationship between the object and the right camera in Fig. 8 to define the trackability c_R of the right camera on a object:

$$c_R = \frac{1}{T}\int_0^T \frac{\sqrt{{}^{R}x_{\hat{M}}^2 + {}^{R}y_{\hat{M}}^2}}{{}^{R}z_{\hat{M}}}dt \tag{16}$$

here T is the time used for tracking visual servoing experiment, and the trackability of the left camera and the end-effector can be calculated in the similar way, it is easy to see that when the object is always keeping in the center of the sight of the right camera, $c_R = 0$, in this case, we have the best trackability of the right camera. Then the controller

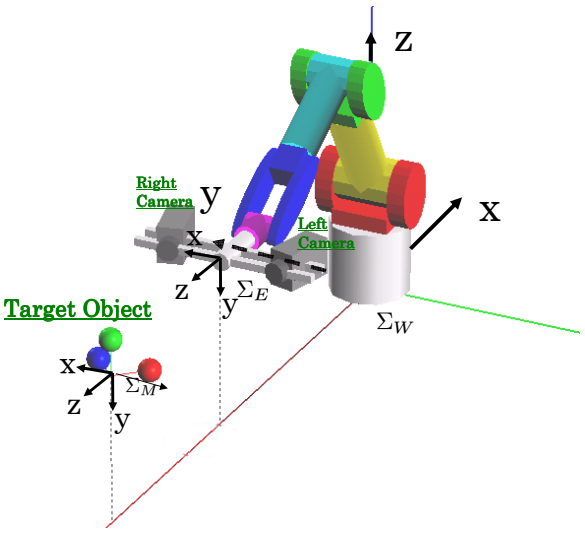

Fig. 9. Object and the visual-servoing system

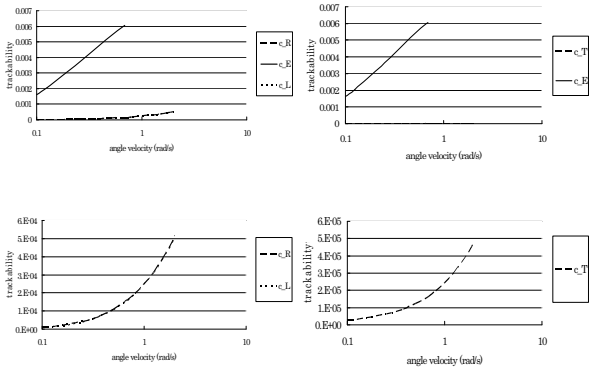

Fig. 10. trackability of the end effector and the cameras

of eye-visual servoing is given by

$$\dot{q}_8 = \boldsymbol{K}_{P_T}(\boldsymbol{q}_{8d} - q_8) + \boldsymbol{K}_{D_T}(\dot{q}_{8d} - \dot{q}_8), \tag{17}$$
$$\dot{q}_9 = \boldsymbol{K}_{P_R}(\boldsymbol{q}_{9d} - q_9) + \boldsymbol{K}_{D_R}(\dot{q}_{9d} - \dot{q}_9), \tag{18}$$
$$\dot{q}_{10} = \boldsymbol{K}_{P_L}(\boldsymbol{q}_{10d} - q_{10}) + \boldsymbol{K}_{D_L}(\dot{q}_{10d} - \dot{q}_{10}) \tag{19}$$

where $\boldsymbol{K}_{P_T}$, $\boldsymbol{K}_{D_T}$, $\boldsymbol{K}_{P_L}$, $\boldsymbol{K}_{D_L}$, $\boldsymbol{K}_{P_R}$, $\boldsymbol{K}_{D_R}$ are positive control gain.

III. EXPERIMENT OF HAND & EYE-VERGENCE VISUAL SERVOING

To verify the effectiveness of the proposed hand & eye visual servoing system, we conduct the simulation of visual servoing to a 3D marker that is composed of a red ball, a green ball and a blue ball as Fig. 9. The radiuses of these three balls are set as 30[mm].

A. experiment condition

To cancel the error caused by the recognition of the object, we will give the position and orientation of the object to the robot directly in the experiment. The initial hand pose is defined as Σ_{E_0}, while the initial object pose is defined as Σ_{M_0}, and the homogeneous transformation matrix from Σ_W to Σ_{M_0} is:

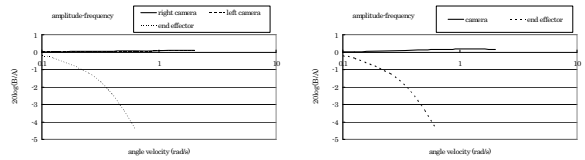

Fig. 11. amplitude-frequency curve of the end-effector and the cameras

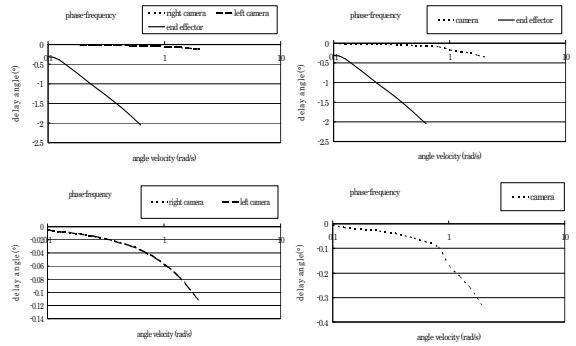

Fig. 12. phase-frequency curve of the end-effector and the cameras

$$ {}^{W}\boldsymbol{T}_{M_0} = \begin{bmatrix} 0 & 0 & -1 & -1410[mm] \\ 1 & 0 & 0 & 0[mm] \\ 0 & -1 & 0 & 355[mm] \\ 0 & 0 & 0 & 1 \end{bmatrix}. \quad (20) $$

to check the properties of the tilt angle and the pan angle of the both cameras, the object will move according to the following two time function seperately,

$$ {}^{M_0}\boldsymbol{\psi}_M = [-300\sin(\omega t)[mm], 0[mm], 0[mm], 0, 0, 0]^T \quad (21) $$
$$ {}^{M_0}\boldsymbol{\psi}_M = [0[mm], 300\sin(\omega t)[mm], 0[mm], 0, 0, 0]^T \quad (22) $$

here, ω is the angular velocity of the motion of the object.

The relation between the object and the desired end-effector is.

$$ \begin{cases} {}^{Ed}x_M(t) = 0 \\ {}^{Ed}y_M(t) = 0 \\ {}^{Ed}z_M(t) = 800[mm] \\ {}^{Ed}\epsilon_{1M}(t) = 0 \\ {}^{Ed}\epsilon_{2M}(t) = 0 \\ {}^{Ed}\epsilon_{3M}(t) = 0 \end{cases} \quad (23) $$

B. experiment Results

We can see the trackability under different angular velocitys in Fig. 10, because the position and orientation of the object are given directly to the robot, and we use the same manipulator controller in eye-vergence system and fixed camera system, the trackability of the end-effector of the eye-vergence system is same to the trackability of the fixed camera system. In Fig. 10 we can see that as the object angular velocity increase the trackability also increase, and when the ω in (21) and (22) get to 0.6908 rad/s the fixed camera system will lose the object in its sight while in eye-vergence system the cameras can always direct to the object and keep the object in the sight of the cameras, we can know that the eye-vergence system has the better stability than the fixed camera system. We can also see that the trackability of the hand eyes (c_T, c_R and c_L) are smaller than the trackability of the end-effector (c_E) which is also the trackability of the fixed camera system under same ω. From the definition we can know the eye-vergence system has better trackability.

Fig. 11 and Fig. 12 are the amplitude-frequency curve and phase-frequency curve of the fixed camera system and eye-vergence system. In both figures we use the logrithmic scalar of the ω in (21) and (22) as the x-axis. To check the observation ability of the camera we calculate out the point where the camera is gazing at. The gazing point of the right camera expressed in the world frame ${}^{W}\boldsymbol{p}_{GR}$ as it is shown in Fig. 8 and Fig. 9 can be calculated as follow:

$$ {}^{W}x_{GR} = {}^{W}x_E + {}^{E}z_{\hat{M}} \quad (24) $$
$$ {}^{W}y_{GR} = {}^{W}y_E - l_{8R} - {}^{E}z_{\hat{M}}\tan q_9 \quad (25) $$
$$ {}^{W}z_{GR} = {}^{W}z_E + {}^{E}z_{\hat{M}}\tan q_8 \quad (26) $$

here, ${}^{W}x_{GR}$, ${}^{W}y_{GR}$, ${}^{W}z_{GR}$ are the three elements of ${}^{W}\boldsymbol{p}_{GR}$. The gazing point of the left camera can be calculated in the similar way. The position of the end-effector and the gazing points of the cameras on y-axis of the world frame can be approximately expressed as a function $Bsin(\omega t+\phi)$, so the swing of the end-effector of the fixed camera system and the gazing point of the cameras is B, and the swing of motion of the object is A. We set $20\log\frac{B}{A}$ as the y-axis of the amplitude-frequency curve. In Fig. 11, we can see as the angular velocity of the object increase, $20\log\frac{B}{A}$ of the end effector will also decrease, which means the swing of the motion of the end-effector becomes smaller, while the $20\log\frac{B}{A}$ of the gazing points of the cameras always keep near to 0, which means the swing of the motion of the gazing point is near to 300[mm], in fact the the difference between the swing of the motion of the gazing point and the motion of the object in our experiment is smaller than 1% . In (21) for the motion function of the object in y-axis of the world frame is $300sin(\omega t)$[mm], while, In (22) the motion function of the object in z-axis of the world frame is $(355-300sin(\omega t))$[mm], so ϕ in the motion function of the end-effector and hand-eye cameras can be considered as the delay phase, we use the ϕ of the end-effector and the gazing points of the cameras as the y-axis of the phase-frequency figure as Fig. 12, from this figure we can see that the eye-vergence system has smaller delay phase which means it will observe the object better.

IV. Conclusion

In this paper, we put forward a new concept to evaluate the observation ability on a moving object of visual servoing system, and introduce the importance of it. To check the trackability of eye-vergence visual servoing system. In eye-vergence system the controller includes two loops: an outer loop for conventional visual servoing that direct a manipulator toward a target object and an inner loop for active motion of binocular camera for accurate and broad observation of the target object. In the experiment we compare the trackability, amplitude-frequency and phase-frequency curves of

the cameras of the eye-vergence system and the fixed camera system under moving object with different angular velocity, and get the conclusion that the trackability and stability of the eye-vergence system is better than that of the fixed-camera system.

REFERENCES

[1] S.Hutchinson, G.Hager, and P.Corke, "A Tutorial on Visual Servo Control", IEEE Trans. on Robotics and Automation, vol. 12, no. 5, pp. 651-670, 1996.

[2] E.Malis, F.Chaumentte and S.Boudet, "2-1/2-D Visual Servoing", IEEE Trans. on Robotics and Automation, vol. 15, no. 2, pp. 238-250, 1999.

[3] Amei massoud Farahmand, Azad Shademan, Martin Jägersand, Csaba szepesvári "Model-based and Model-free Reinforcement Learning for Visual Servoing" IEEE International Conference on Robotics and Automation Kobe, Japan, May 12-17, 2009

[4] Toshifumi Hiramatsu, Takanori Fukao, Keita Kurashiki, Koichi Osuka "Image-based Path Following Control of Mobile Robots with Central Catadioptric Cameras" IEEE International Conference on Robotics and Automation Kobe, Japan, May 12-17, 2009

[5] Omar Tahri, Youcef Mezouar "Generic Decoupled Image-Based Visual Servoing for Cameras Obeying the Unified Projection Model" IEEE International Conference on Robotics and Automation Kobe, Japan, May 12-17, 2009

[6] Dae-Jin Kim, Ryan Lovelett, and Aman Behal "Eye-in-Hand Stereo Visual Servoing of an Assistive Robot Arm in Unstructured Environments" IEEE International Conference on Robotics and Automation Kobe, Japan, May 12-17, 2009

[7] W. Song, M. Minami, Y. Mae and S. Aoyagi, "On-line Evolutionary Head Pose Measurement by Feedforward Stereo Model Matching", IEEE Int. Conf. on Robotics and Automation (ICRA), pp.4394-4400, 2007.

[8] J. Stavnitzky, D. Capson, "Mutiple Camera Model-Based 3-D Visual Servoing", IEEE Trans. on Robotics and Automation, vol. 16, no. 6, December 2000.

[9] C. Dune, E. Marchand, C. leroux, "One Click Focus with Eye-in-hand/Eye-to hand Cooperation", IEEE Int. Conf. on Robotics and Automation (ICRA), pp.2471-2476, 2007.

[10] Omar Tahri and Francois Chaumette, "Point-Based and Region-Based Image Moments for Visual Servoing of Planar Objects", IEEE Tran. on Robotics, vol. 21, no. 6, Dec 2005.

[11] Tarek Hamel and Robert Mahony, "Visual Servoing of an Under-Actuated Dynamic Rigid-Body System: An Image-Based Approach", IEEE Trans. on Robotics and Automation, VOL. 18, NO. 2, APRIL 2002.

[12] Tomoyuki Shiozaki, Toshiyuki Murakami. "Trackability Based Motion Control in Mobile Hand-Eye System". SICE-ICASE International Joint Conference 2006, pp.5304-5309.

[13] Wei Song, Mamoru Minami,"Stability / Precision Improvement of 6-DoF Visual Servoing by Motion Feedforward Compensation and Experimental Evaluation", IEEE International Conference on Robotics and Automation (ICRA), pp.722-729, 2009

[14] Tsuneo Yoshikawa *Foundations of Robotics Analysis and Control*, ISBN 0-2622-4028-4.

[15] W. Song, M. Minami, S. Aoyagi, "On-line Stable Evolutionary Recognition Based on Unit Quaternion Representation by Motion-Feedforward Compensation", International Journal of Intelligent Computing in Medical Sciences and Image Processing (IC-MED) Vol. 2, No. 2, Page 127-139 (2007).

[16] B.Siciliano and L.Villani: *Robot Force Control*, ISBN 0-7923-7733-8.